Wave Motions in Stratified Fluids by a Translating Plate

Sang Woo Joo*, Min Soo Park
School of Mechanical Engineering, Yeungnam University, Gyeongsan 712-749, Korea

Surface and interfacial waves in two superposed horizontal inviscid fluids of finite depths are studied. The flow is induced by translating a vertical rigid plate with a prescribed velocity. Analytical solutions that accurately predict the motion of the free surface and the interface are obtained by using a small-Froude-number approximation. Three different velocities of the plate are considered, while flows induced by any arbitrary motion of the plate can be easily analyzed by a linear superposition of the solutions obtained. It is shown that pinching of the upper layer can occur for a sufficiently thin upper layer, which leads to its rupture into small segments. Other interesting phenomena, such as primary and secondary wiggles generated on the interface near the wavemaker, are discussed.

Key Words : Wave Motion, Inviscid Flow, Stratified Fluid

Nomenclature

h : Ratio of lower to upper layer thickness
g : Gravitational acceleration
T : Dimensionless surface tension
U : Time-dependent velocity of the plate
u : Dimensionless plate velocity
α : Froude number
η : Surface elevation
ρ : Ratio of lower to upper layer density
ϕ : Velocity potential
σ : Surface tension coefficient
ω : Dimensionless frequency of plate translation

1. Introduction

Analyzing flows with a free surface can be more demanding than those with fixed boundaries due to the extra effort of determining the location of the free surface which is unknown a priori. Additional difficulties exist when a partially submerged structure translates in the fluid because the flow near the contact line that the free surface makes with the structure usually is not scaled with a fixed length scale of the problem.

A generic problem for the flow with a free surface and a surface-piercing body is the wavemaker problem, where a vertical plate translates in an inviscid horizontal fluid with a prescribed velocity. Since the early work by Peregrine (1972), who reported the apparent singularity at the contact line, many researchers, including Chwang (1983) and Lin (1984), have contributed to this disputable problem. The first local solution valid near the contact line is obtained by Roberts (1987), and a uniformly valid solution that matches with the self-similar local solution near and the outer solution away from the contact line is presented by Joo et al.(1990).

Wavemaker problems for stratified fluids can be quite involved owing to the added complexities with the internal or interfacial waves. Rhodes-Robins (1994) and Shrief et al.(2003), among others, report on wave motions in a two-layered liquid. Joo and Park (2005) extend the initial wavemaker problem of Joo et al.(1990) to two layers with infinite depth, and show uniformly valid solutions for the free surface and the interface motions.

* Corresponding Author,
E-mail : swjoo@yumail.ac.kr
TEL : +82-53-810-2440; **FAX** : +82-53-813-3703
School of Mechanical Engineering, Yeungnam University, Gyeongsan 712-749, Korea. (Manuscript **Received** November 17, 2005; **Revised** March 13, 2006)

In this study flows induced by a vertical wavemaker in two fluid layers of finite depths are studied. The rigid bottom and the wavemaker reaching the bottom prevent the displaced fluids from leaving behind the translating wavemaker, and thus generate qualitatively different dynamics from the ones in infinite depth with a finite wavemaker draft. We report the resulting flow of the two layers with precise predictions of the free surface and the interface motions.

2. Formulation

Formulation of the problem is done by a straightforward extension of that for a single-layer fluid of Joo et al.(1990), and is presented with a minimal detail below. Descriptions obvious from figures or the nomenclature provided will not be repeated in the text.

A two dimensional inviscid flow is generated from rest by a horizontal motion of the wavemaker, as shown in Fig. 1. Conservation of mass for each layer gives equations for the velocity potentials as

$$\phi^{(1)}_{xx}+\phi^{(1)}_{yy}=0 \text{ for } x>s(t),\ -1<y<\eta^{(1)} \quad (1)$$

$$\phi^{(2)}_{xx}+\phi^{(2)}_{yy}=0 \text{ for } x>s(t),\ \eta^{(1)}<y<-1 \quad (2)$$

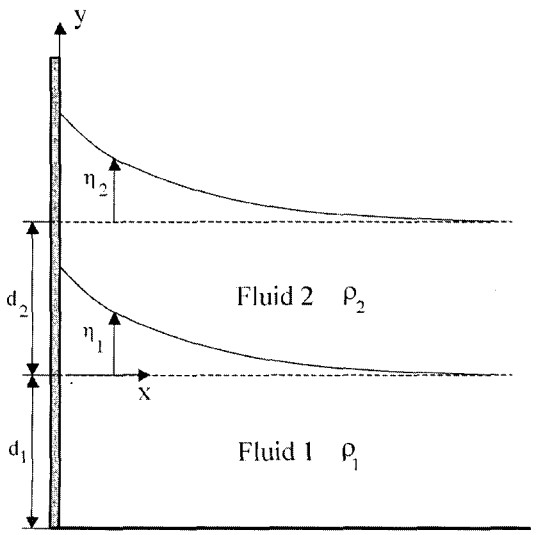

Fig. 1 Configuration for a two-layer wavemaker problem

where $(gd_1)^{1/2}$ and d_1 are used as the velocity and the length scales, respectively. The Cartesian coordinate system (x, y) is located at the initial wavemaker position, so that the location of the wavemaker is at $x=s(t)$.

Boundary conditions on rigid surfaces are

$$\phi^{(1)}_x=au(t) \text{ on } x=s(t) \quad (3)$$

$$\phi^{(2)}_x=au(t) \text{ on } x=s(t) \quad (4)$$

$$\phi^{(1)}_x=0 \text{ on } y=-1 \quad (5)$$

where the Froude number a is defined depending on the prescribed wavemaker velocity.

At the interface between the upper and the lower fluids, the normal-stress jump, continuity of velocity, and the kinematic condition are imposed:

$$\phi^{(1)}_t+\frac{1}{2}(\phi^{(1)2}_x+\phi^{(1)2}_y)+\eta^{(1)} -\rho\left[\phi^{(2)}_t+\frac{1}{2}(\phi^{(2)2}_x+\phi^{(2)2}_y)+\eta^{(1)}\right] =\frac{T_1\eta^{(1)}_{xx}}{(1+\eta^{(1)2}_x)^{\frac{3}{2}}} \text{ on } y=\eta^{(1)} \quad (6)$$

$$\phi^{(1)}_y-\phi^{(1)}_x\eta^{(1)}_x=\phi^{(2)}_y\phi^{(2)}_x\eta^{(1)}_x \text{ on } y=\eta^{(1)}$$
$$\phi^{(1)}_y=\eta^{(1)}_t+\phi^{(1)}_x\eta^{(1)}_x \text{ on } y=\eta^{(1)} \quad (7)$$

where the nondimensional interfacial tension

$$T_1=\frac{\alpha_1}{\rho_1 g d^2} \quad (8)$$

At the free surface between the upper fluid and the air, the boundary conditions are

$$\phi^{(2)}_t+\frac{1}{2}(\phi^{(1)2}_x+\phi^{(2)2}_y)+\eta^{(2)}=\frac{T_2\eta^{(2)}_{xx}}{(1+\eta^{(2)2}_x)^{\frac{3}{2}}} \text{ on } y=h+\eta^{(2)} \quad (9)$$

$$\phi^{(2)}_y=\eta^{(2)}_t+\phi^{(2)}_x\eta^{(2)}_x \text{ on } y=h+\eta^{(1)} \quad (10)$$

where

$$T_2=\frac{\alpha_2}{\rho_2 g d^2} \quad (11)$$

Initially, both fluids are at rest and the interfaces are planar, so that

$$\phi^{(1)}=\phi^{(2)}=0 \text{ when } t\leq 0 \quad (12)$$

$$\eta^{(1)}=\eta^{(2)}=0 \text{ when } t\leq 0 \quad (13)$$

It is assumed here that static contact angles are 90 degrees at both contact lines.

3. Analysis

We expand all dependent variables in simple power series in α, and substitute these into the governing system above. The leading-order equations resulting from this small-Froude-number asymptotics are, after dropping the order indices,

$$\phi^{(1)}_{xx}+\phi^{(1)}_{yy}=0 \text{ for } x>0,\ -1<y0 \tag{14}$$

$$\phi^{(1)}_{xx}+\phi^{(2)}_{yy}=0 \text{ for } x>0,\ 0<y<h \tag{15}$$

$$\phi^{(1)}_{x}=u(t) \text{ on } x=0 \tag{16}$$

$$\phi^{(2)}_{x}=u(t) \text{ on } x=0 \tag{17}$$

$$\phi^{(1)}_{x}=0 \text{ on } y=-1 \tag{18}$$

$$\eta^{(1)}_{t}=\phi^{(1)}_{y} \text{ on } y=0 \tag{19}$$

$$\phi^{(1)}_{y}=\phi^{(2)}_{y} \text{ on } y=0 \tag{20}$$

$$\phi^{(1)}_{t}+\eta^{(1)}-\rho(\phi^{(2)}_{t}+\eta^{(1)})-T_1\eta^{(1)}_{xx}=0 \text{ on } y=0 \tag{21}$$

$$\eta^{(2)}_{t}=\phi^{(2)}_{y} \text{ on } y=h \tag{22}$$

$$\phi^{(2)}_{t}+\eta^{(2)}-T_2\eta^{(2)}_{xx}=0 \text{ on } y=h \tag{23}$$

In solving the above system for $\phi^{(1)}$, $\phi^{(2)}$, $\eta^{(1)}$, and $\eta^{(2)}$, we first decompose $\phi^{(1)}$ into three parts:

$$\phi^{(1)}=2u(t)\sum_{n=0}^{\infty}\frac{1}{k_n^2}e^{-k_nx}\sin k_n - \frac{2u(t)}{\pi}\int_0^{\infty}\frac{\cosh(ky+k)}{k^2\cosh(k)}\cos kx\,dk + \phi^{*(1)}(x,\ y,\ t) \tag{24}$$

where $k_n=(n+0.5)\pi$. The series and the Fourier integral on the right-hand side satisfy the Laplace equation and all boundary conditions except on the interface, where it becomes zero. The remaining part $\phi^{*(1)}$ then enables the solution to satisfy the interface conditions. Similarly for $\phi^{(2)}$ we set

$$\phi^{(2)}=-\frac{4u(t)}{h}\sum_{m=0}^{\infty}\frac{1}{k_m^2}e^{-k_mx}\sin k_my+\phi^{*(1)} - \frac{2u(t)}{\pi}\int_0^{\infty}\frac{\cosh(ky-ky/2)}{k^2\cosh(kh/2)}\cos kx\,dk + \phi^{*(2)}(x,\ y,\ t) \tag{25}$$

where $k_m=(2m-1)\pi/h$. The series and the Fourier integral, together satisfy the boundary conditions on the wavemaker and at the interface between the upper and the lower fluids.

Substituting the above expressions into the governing system reveals that $\phi^{*(1)}$ and $\phi^{*(2)}$ both satisfy the Laplace equation,

$$\phi^{*(1)}_{xx}+\phi^{*(1)}_{yy}=0 \text{ for } x>0,\ -1<y<0 \tag{26}$$

$$\phi^{*(2)}_{xx}+\phi^{*(2)}_{yy}=0 \text{ for } x>0,\ 0<y<h \tag{27}$$

homogeneous boundary conditions on the wavemaker,

$$\phi^{*(1)}_{x} \text{ on } x=0 \tag{28}$$

$$\phi^{*(2)}_{x} \text{ on } x=0 \tag{29}$$

and homogeneous boundary condition on the bottom surface,

$$\phi^{*(1)}_{y} \text{ on } y=-1 \tag{30}$$

The decompositions Eqs. (24) ~ (25) also guarantee the homogeneous boundary condition

$$\phi^{*(2)}_{y} \text{ on } y=0 \tag{31}$$

Considering these, we seek for the solutions $\phi^{(1)}$ and $\phi^{(2)}$ as Fourier cosine integrals:

$$\phi^{*(1)}=\int_0^{\infty}A(k,\ t)\cosh[k(y+1)]\cos kx\,dk \tag{32}$$

$$\phi^{*(2)}=\int_0^{\infty}C(k,\ t)\cosh ky\cos kx\,dk \tag{33}$$

The solutions for $\eta^{(1)}$ and $\eta^{(2)}$ then are also in Fourier integrals:

$$\eta^{(1)}=\int_0^{\infty}B(k,\ t)\cos kx\,dk \tag{34}$$

$$\eta^{(2)}=\int_0^{\infty}D(k,\ t)\cos kx\,dk \tag{35}$$

The Fourier coefficients A, B, C, and D are obtained by applying the remaining four boundary conditions, one dynamic and one kinematic conditions each for the interface ($y=0$) and the free surface ($y=h$).

In obtaining appropriate equations for the Fourier coefficients by eliminating Fourier integrations, it is necessary to note the following identities:

$$\sum_{n=0}^{\infty}\frac{1}{k_n}e^{-k_nx}=-\frac{1}{\pi}\ln\tanh\left(\frac{\pi x}{4}\right) \tag{36}$$

$$-\ln\tanh\left(\frac{\pi x}{4}\right)=\int_0^{\infty}\cos kx\tanh k\frac{dk}{k} \tag{37}$$

as in Gradshteyn & Ryzhik (1980). From the condition Eq. (19) we then get

$$k\sinh kA(k,\ t)=B_t(k,\ t) \tag{38}$$

while the condition Eq. (20) gives

$$-\frac{2(1-\rho)u'(t)}{\pi k^2}+(1-\rho)A_t(k,\ t)\cosh k -\rho C_t(k,\ t)+(1-\rho+T_1k^2)B(k,\ t)=0 \tag{39}$$

The kinematic condition Eq. (21) yields

$$kA(k,\ t)\sinh(kh+k) +kC(k,\ t)\sinh(kh)=D_t \tag{40}$$

and finally the dynamic condition Eq. (22) gives

$$-\frac{2u'(t)}{\pi k^2}+\cosh(kh+k)A_t(k,\ t) +\cos(kh)C_t+(1+T_2k^2)D(k,\ t)=0 \tag{41}$$

The Fourier coefficients B and D can be eliminated between equations Eqs. (38) ~ (39) and Eqs. (40) ~ (41), respectively, yielding equations for A and C. We then eliminate C to obtain a single fourth-order ordinary differential equation for A:

$$a_1A_{tttt}+a_2A_{tt}+a_3A=a_N \tag{42}$$

where

$$a_1=\cosh k\cosh(kh)+\rho\sinh k\sinh(kh) \tag{43}$$

$$a_2=k(1-\rho T_1k^2)\sinh k\cosh(kh) +k(1+T_2k^2)[\rho\sinh\cosh(kh) +\cosh k\sinh(kh)] \tag{44}$$

$$a_3=k^2(1-\rho+T_1k^2)(1+T_2k^2)\sinh k\sinh(kh) \tag{45}$$

$$a_N=\frac{2\gamma_2(1-\rho)u''(t)}{\pi k\cosh k}\tanh(kh) +\frac{2u''''(t)}{\pi k^2\cosh k}\left(1-\rho+\frac{\rho}{\cosh(kh)}\right) \tag{46}$$

Eq. (42) has a general solution

$$A=A_p(k,\ t)+c_1(k)\sin(\beta_1t)+c_2(k)\cos(\beta_1t) +c_1(k)\sin(\beta_2t)+c_4(k)\cos(\beta_2t) \tag{47}$$

where

$$\beta_1=\left(\frac{a_2-\sqrt{a_2-4a_1a_3}}{2a_1}\right)^{1/2}$$
$$\beta_2=\left(\frac{a_2+\sqrt{a_2-4a_1a_3}}{2a_1}\right)^{1/2} \tag{48}$$

Here, A_p is a particular solution of Eq. (42) for a given q, and c_i's (i=1,2,3,4) are determined from the initial conditions.

The initial conditions for interface elevations $\eta^{(1)}$ and $\eta^{(2)}$ can be converted into those for $\phi^{(1)}$, and $\phi^{(2)}$ through Eq. (21) and Eq. (22). The appropriate initial conditions are then

$$\phi^{(1)}=0 \text{ on } \phi_t^{(1)}=\rho\phi_t^{(2)} \tag{49}$$

at y=0 and

$$\phi^{(2)}=0 \text{ on } \phi_t^{(2)}=0 \tag{50}$$

at $y=h$. These conditions are easily converted in turn into those for $A(k,\ 0)$. The solution for $A(k,\ t)$ then is completely determined, after which that for $C(k,\ t)$ and consequently those for B and D are obtained; the time-dependent configurations for the interface and the free surface are determined in terms of Fourier integrals.

We note that the wavemaker velocity is not restricted by the solution method. In this study we consider three different wavemaker motions, constant acceleration, constant velocity, and periodic oscillation. The constant acceleration provides insight into the start-up behavior of wavemaker-induced flows, as many time-dependent motions can be approximated for small time as ramp velocity as a first-order approximation. The constant velocity allows us to look into the behaviors for impulsive motions and for long time because the wavemaker speed is bounded. It can model the final motions of many translating surface-piercing objects. The oscillatory motion is important for itself, but can become more useful because any general wavemaker motion can be described by superposing harmonic motions with different frequency.

4. Constant Acceleration

When the wavemaker starts from rest and increases linearly in time with a constant acceleration Q, the Froude number α and the dimensionless wavemaker velocity become

$$\alpha=\frac{Q}{g} \text{ and } u(t)=t \tag{51}$$

respectively. For the present analysis to be valid, the acceleration of the wavemaker must be much smaller than the gravitational acceleration. From the initial conditions, we get

$$A(k, 0)=0 \tag{52}$$

$$A_t(k, 0)=\frac{2}{\pi k^2\lambda\cos k}\left[1-\rho+\frac{\rho}{\cosh kh}\right] \tag{53}$$

$$A_{tt}(k, 0)=0 \tag{54}$$

$$\begin{aligned}A_{ttt}(k, 0)=&-\frac{2}{\pi k\lambda^2\cosh k}[\gamma_2\tanh k(\rho^2\tanh^2(kh)\\&-\rho^2-\rho\tanh^2(kh)+1)]\\&-\frac{2\gamma_1(\rho+1)\tanh k}{\pi k\lambda^2\cosh k}\\&-\frac{2\rho[\gamma_2(\rho\tanh k+\tanh(kh))+\gamma_1\tanh k]}{\pi k\lambda^2\cosh k\cosh(kh)}\end{aligned} \tag{55}$$

where $\lambda=1+\rho\tanh k\tanh(kh)$, $\gamma_1=1-\rho+k^2T_1$, and $\gamma_2=1+k^2T_2$.

Figure 2 shows the interface configurations at a small time ($t=0.1$) when two fluid layers are of the same thickness ($h=0$). The density ratio ρ is varied from 0.01 (upper fluid much lighter) to 0.99 (upper and lower fluid similar in density). Considering that the density is here the only physical property that distinguishes the two inviscid fluids and that only hydrodynamically stable stratifications are required for the initial conditions taken, we do not take density ratios equal or higher than unity. When the density ratio is very small as in Fig. 2(a), the upper fluid behaves like passive air for the lower fluid, so that the motion of the lower fluid is similar to that of a single fluid layer (no upper fluid). The configuration of the interface approaches that obtained

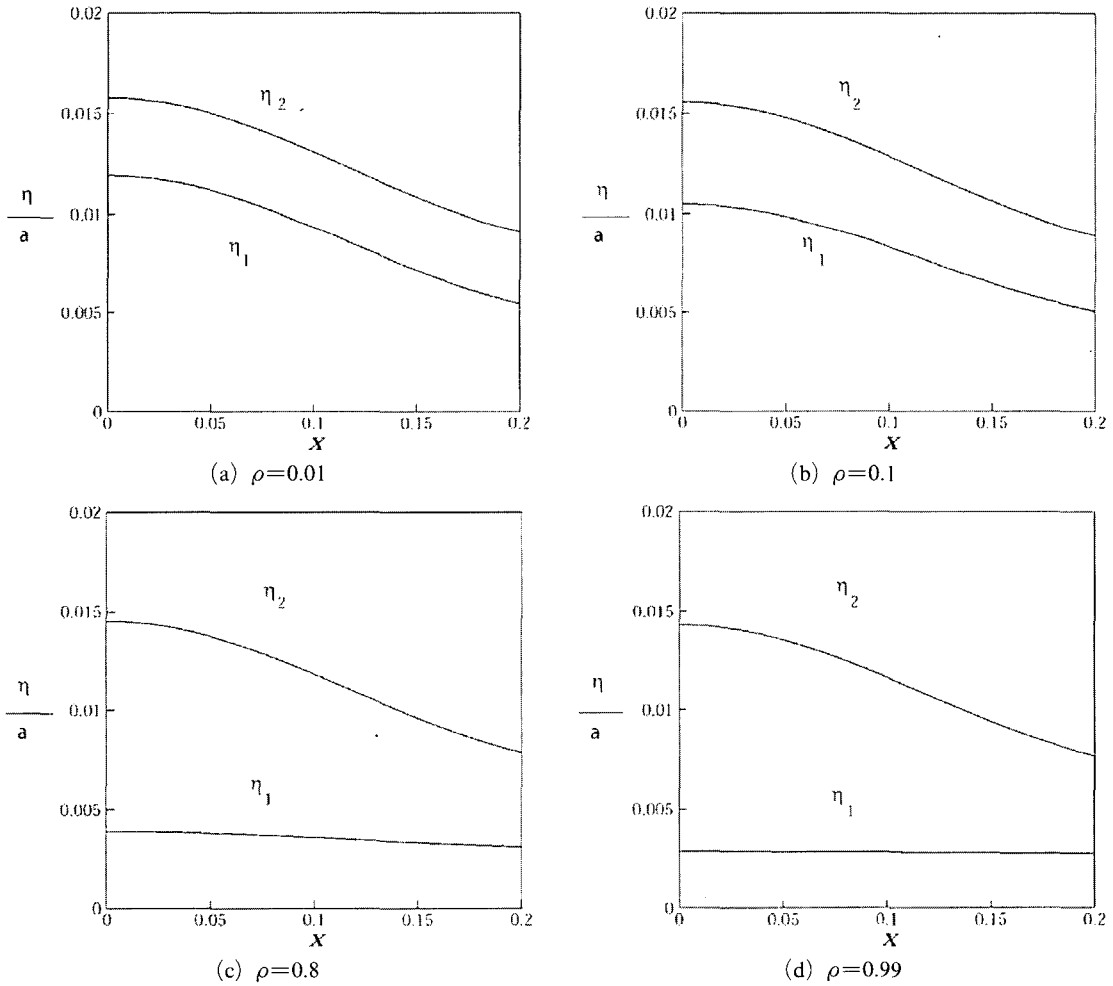

(a) $\rho=0.01$ (b) $\rho=0.1$

(c) $\rho=0.8$ (d) $\rho=0.99$

Fig. 2 Surface configurations for the ramp velocity at $t=0$ for $T_1=2\times10^{-6}$, $T_2=2T_1$, and $h=1$

by Joo et al.(1990). As the density ratio increases, the motion of the interface is decreased, while the free-surface elevation is also decreased. If the density ratio is further increased toward unity, the motion of the interface is further decreased, so that the interface configuration becomes almost planar. The free-surface elevation is also decreased, but its configuration resembles that for a single fluid, with appropriate rescaling of length. The elevation of the free surface (and of the interface) seems to have both upper and lower bounds as the density ratio approaches zero and unity, respectively.

In Fig. 3, the density ratio is fixed at $\rho=0.8$, a representative value for water and a typical petroleum oil. The thickness ratio h is varied from unity to 0.01. As the thickness of the upper fluid decreases, the elevation of the interface becomes more and more pronounced, and for very small h, as in Fig. 3(a), the interface configuration again recovers that of a single fluid. The free-surface elevation on the other hand decreases with the decrease in the thickness ratio.

Figure 4 shows the free-surface and interface configurations at two different times for three different combinations of interfacial tension. At a given time, the elevations at the contact-line are lower with the increase of the surface tension. Away from the wavemaker the effect of surface tension becomes less important, and the surface configurations for all values of surface tension become identical. The figures for $t=1$ clearly

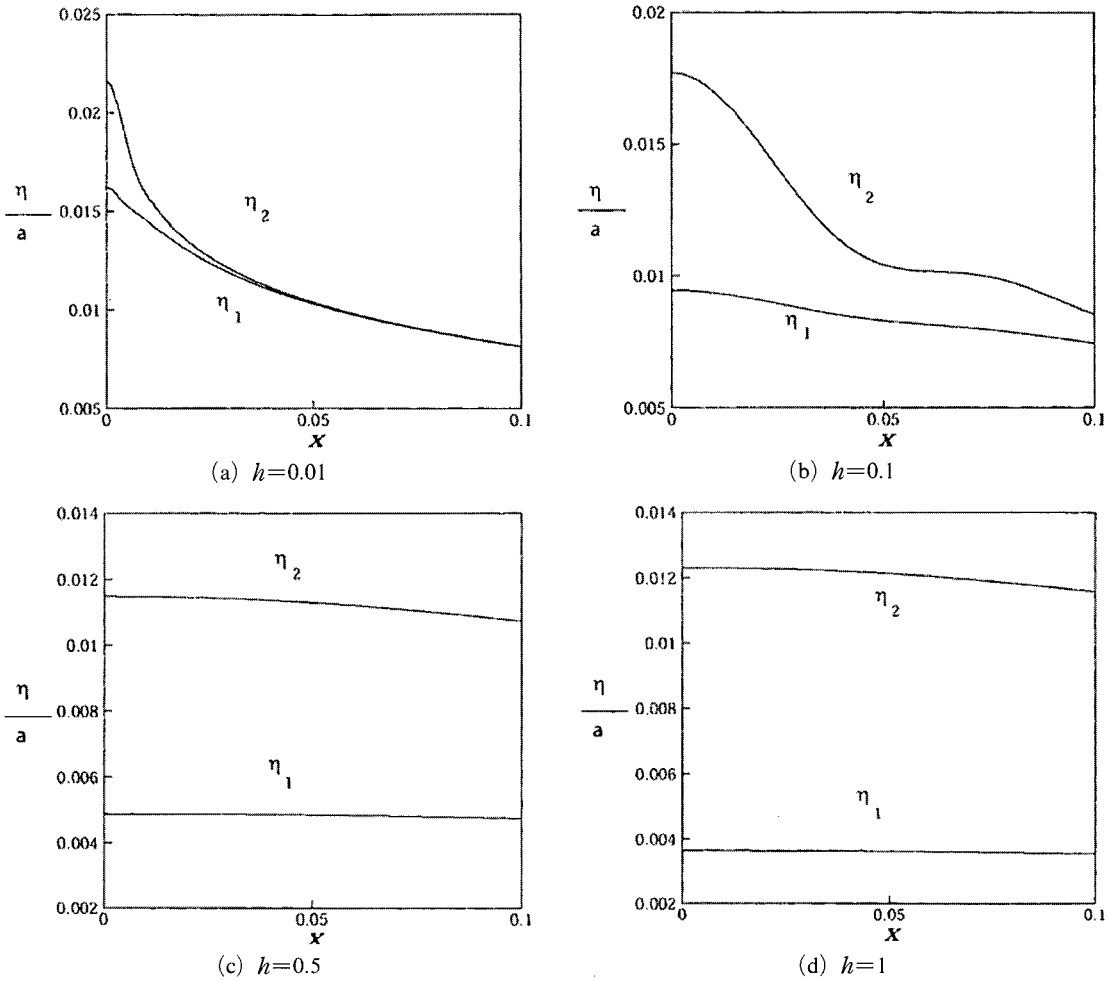

Fig. 3 Surface configuration for the ramp velocity when $t=0.1$ for $T_1=2\times10^{-6}$, $T_2=2T_1$, and $\rho=0.8$

show the generation and propagation of small-scale capillary waves near the wavemaker. The propagation rate appears to increase with the surface tension. These effects become more obvious for a step motion of the wavemaker shown below.

In Fig. 5, the contact-line elevations (η_i at $x=0$) are plotted against time for various combinations of thickness ratio, density ratio, and surface tension. Fig. 5(a) shows monotonic increase in the elevations for both contact-lines. For this particular case, the contact-line elevation for the free surface always exceeds that for the interface. Fig. 5(b) shows the effect of thickness ratio on the contact-line elevation for the free surface. Increase in the relative thickness of the upper layer provides increase in the contact-line elevation, which becomes more conspicuous as time progresses. The effect of density ratio is plotted in Fig. 5(c). As seen in previous figures, the contact-line elevation for the interface decreases as the density of the upper layer increases. In Fig. 5(d) the difference in the two contact-line elevations is plotted for three different combinations of surface tension. For all cases shown, the contact-line elevation for the free surface is always higher. For small time this extra elevation for the free surface decreases with surface tension. At larger times, however, the trend is reversed ; the surface tension promotes the extra contact-line elevation for the free surface.

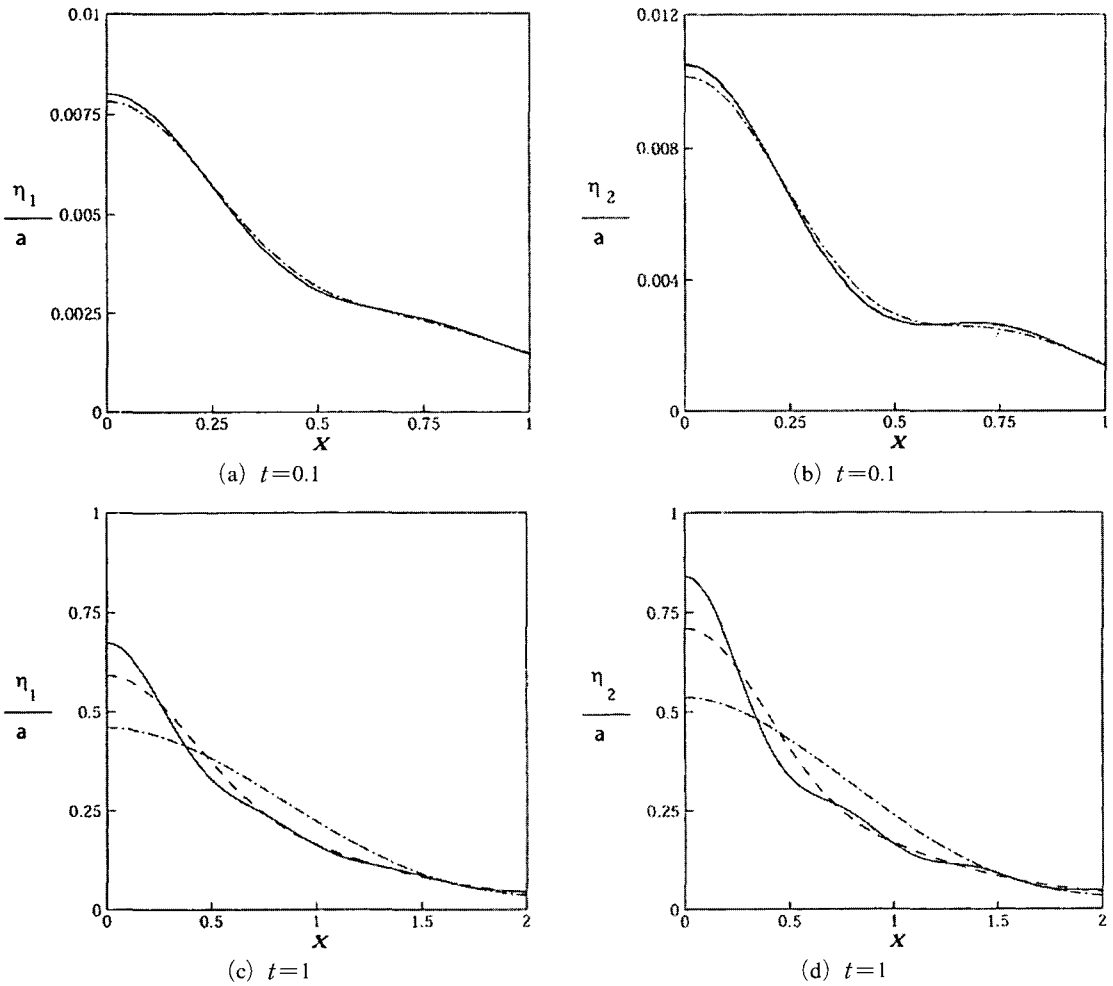

Fig. 4 Surface configurations for the ramp velocity when $\rho=0.8$, $h=0.1$ for $T_1=2\times10^{-6}$ (Solid), $T_1=2\times10^{-2}$ (Dash), $T_1=2\times10^{-1}$ (Dash-Dotted), and $T_2=2T_1$

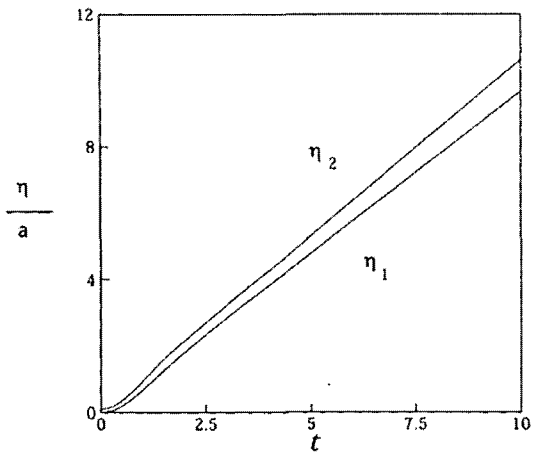

(a) $h=0.1$, $\rho=0.8$, $T_1=2\times10^{-6}$, and $T_2=2T_1$

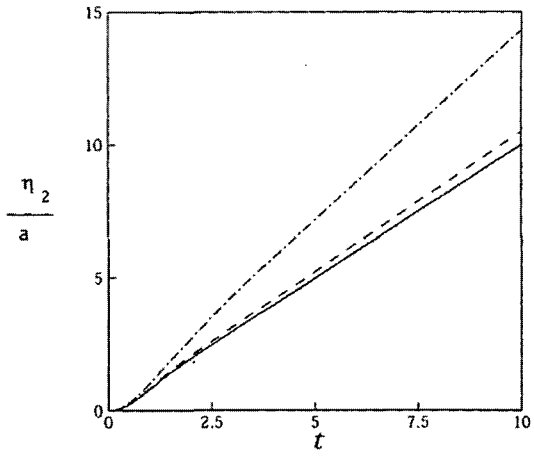

(b) $\rho=0.8$, $T_1=2\times10^{-6}$, and $T_2=2T_1$ with $h=0.001$ (Solid), $h=0.1$ (Dotted), and $h=1$ (Dash-dotted)

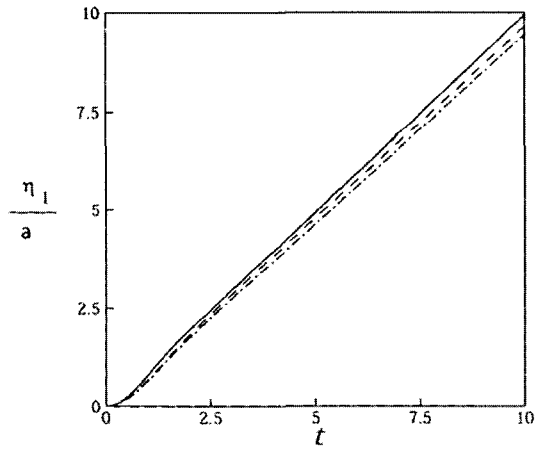

(c) $h=0.1$, $T_1=2\times10^{-6}$, and $T_2=2T_1$ with $\rho=0.001$ (Solid), $\rho=0.8$ (Dash), and $\rho=0.99$ (Dash-dotted)

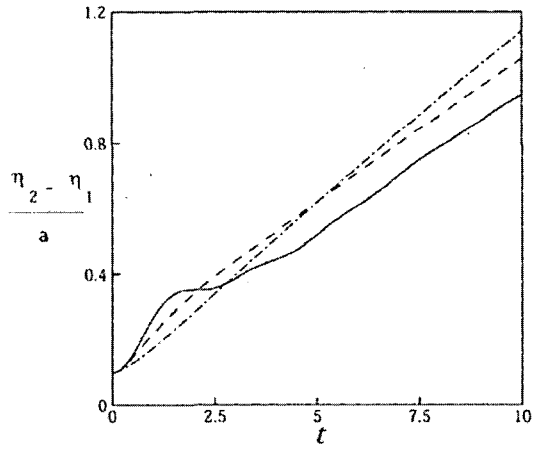

(d) $h=0.1$ and $\rho=0.8$ with $T_1=2\times10^{-6}$ (Solid), $T_1=2\times10^{-2}$ (Dash), $T_1=2\times10^{-1}$ (Dash-Dotted), and $T_2=2T_1$

Fig. 5 Contact-line elevations for the ramp velocity

5. Impulsive Constant Velocity

The Froude number and dimensionless wavemaker velocity become

$$a=\frac{V}{\sqrt{gd_1}} \text{ and } u(t)=1 \tag{56}$$

respectively, for a wavemaker impulsively set in motion with a constant velocity V. The initial conditions are here

$$A(k,0)=\frac{2}{\pi k^2\cosh k} \tag{57}$$

$$A_t(k,0)=0 \tag{58}$$

$$A_{tt}(k,0)=-\frac{2\tanh k}{\pi k\lambda\cosh k}[\gamma_2\rho(\tanh^2(kh)-1)-\gamma_1] -\frac{2\gamma_2\rho\tanh(kh)}{\pi k\lambda\cosh k\cosh(kh)} \tag{59}$$

$$A_{ttt}(k,0)=0 \tag{60}$$

Figure 6 shows the interface and free-surface configurations at a small time ($t=1$) for three different values of the density ratio. For clarity the local configurations near the wavemaker are plotted in a magnified scale in figures (b), (d),

and (f). While other trends are relatively unchanged from those for the ramp velocity, devel-

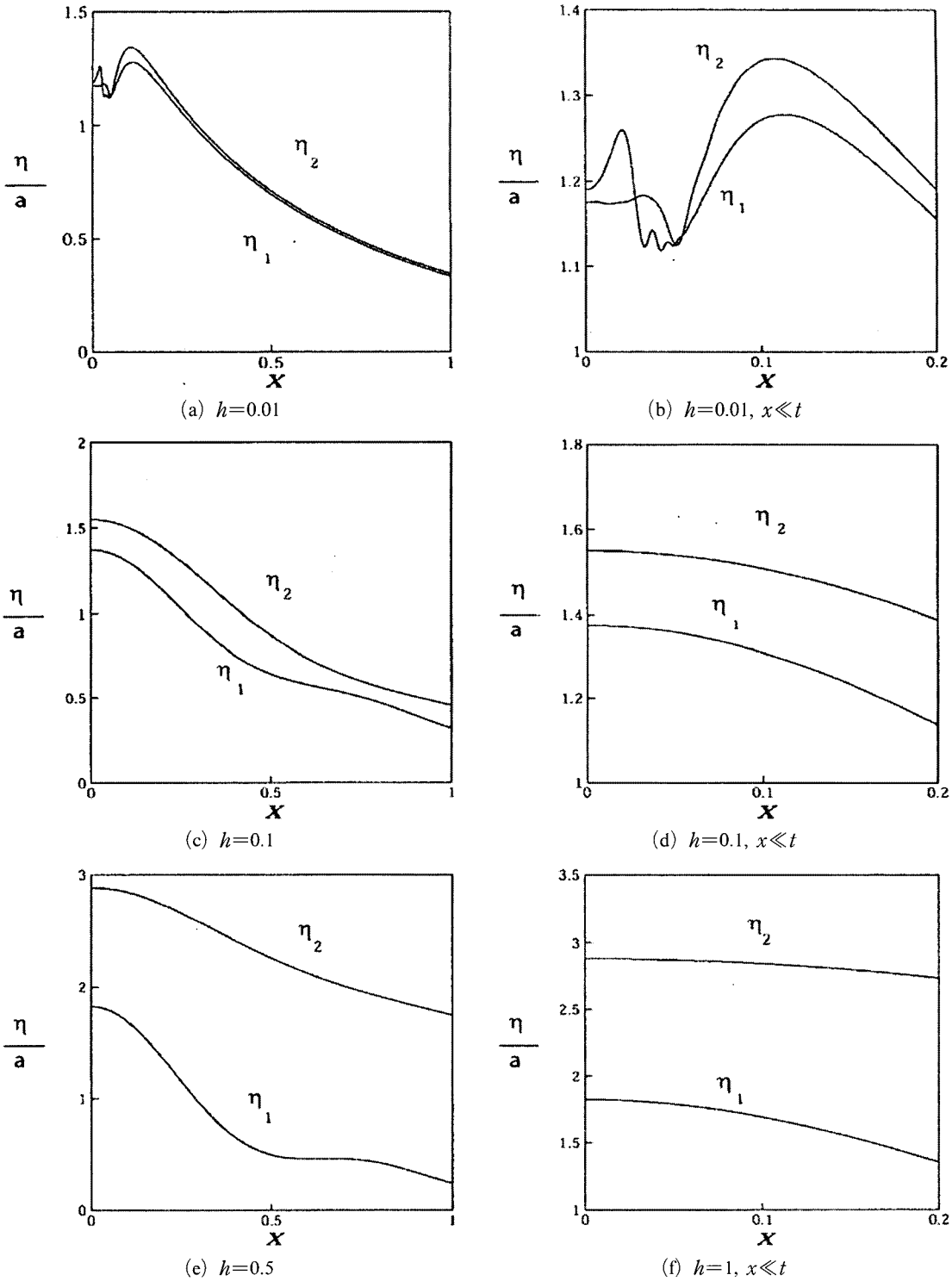

Fig. 6 Surface configurations for the step velocity at $t=1$ when $\rho=0.8$, $T_1=2\times10^{-6}$, and $T_2=2T_1$

opment of wiggles near the wavemaker is notable when the upper layer is sufficiently thin. As seen in Fig. 6(a), for a sufficiently small thickness ratio h the free surface can meet the interface, and a "pinching" can occur that makes the thin upper layer rupture (into isolated drops) at least temporarily.

The wiggles generated by the impulsive motion of the wavemaker can be observed for all values of h as time progresses, as seen in Fig. 7. The thickness ratio is now taken up to $h=2$. Far away from the wavemaker where the wiggles have not reached, the configurations, or wave motions, for the interface and the free surface seem in phase. Near the wavemaker, however, the free surface and the interface exhibit wiggles of their own that do not appear to communicate with each other. This can cause the rupture of the upper layer if it is thin enough, as seen in the previous figure.

In Fig. 8, the contact-line elevations for the interface and the free surface (η_i at $x=0$) are plotted against time for three different combinations of surface tension. The contact-line for the free surface elevates monotonically with time, reaches a maximum, and then oscillates to converge eventually to a finite value. Surface tension retards the initial monotonic increase in contact-line elevation, and decreases the maximum elevation. Surface tension increases the time to reach the maximum elevation, and decreases the frequency of the subsequent oscillations. At a given time the contact-line elevation thus does not mono-

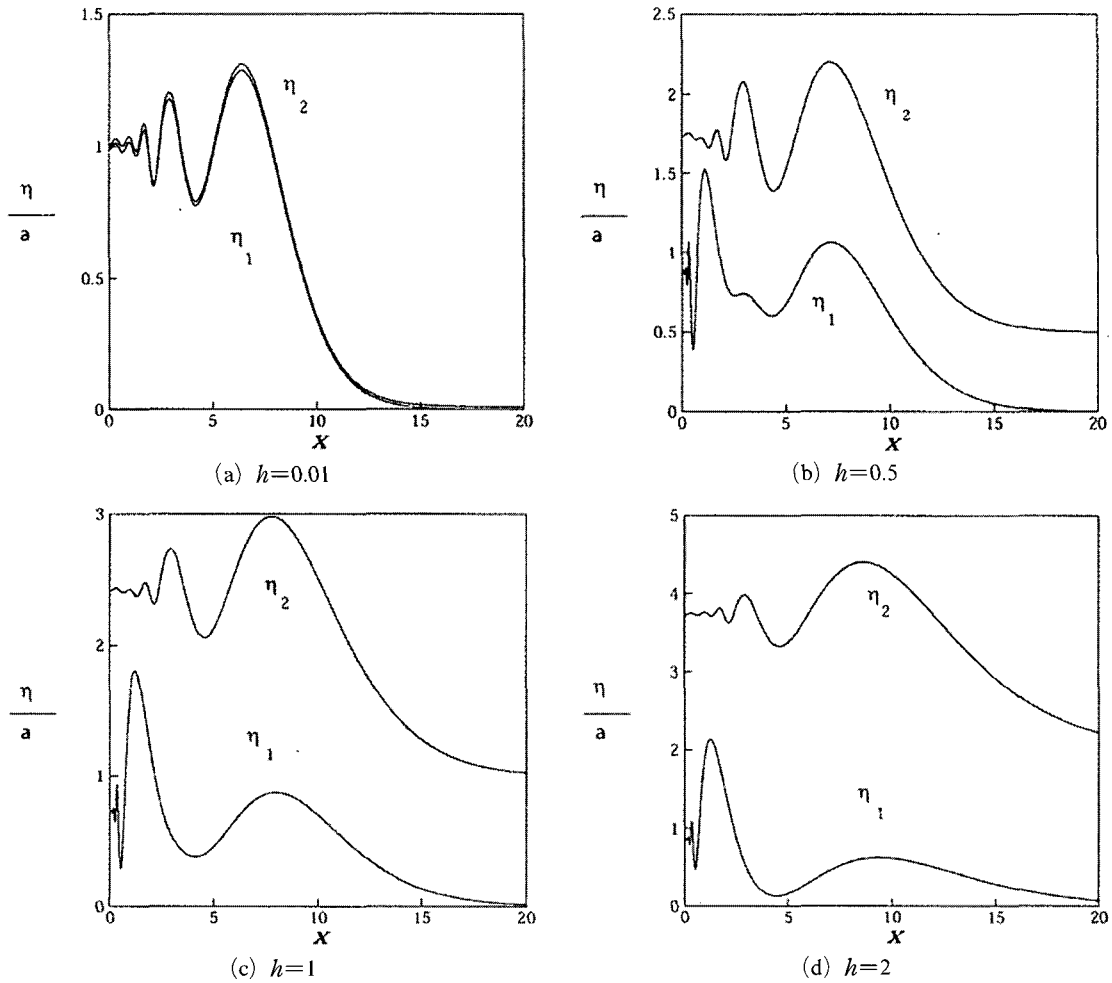

Fig. 7 Surface configurations for the step velocity at $t=10$ when $\rho=0.8$, $T_1=2\times10^{-6}$, and $T_2=2T_1$

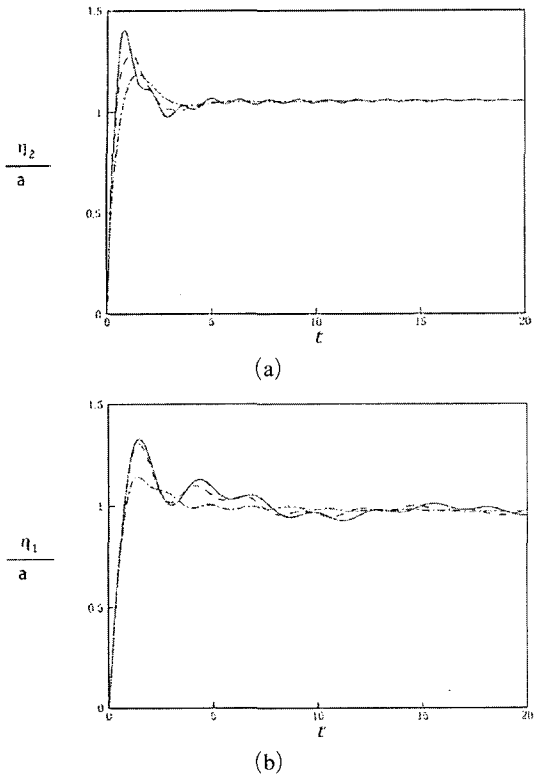

Fig. 8 Contact-line elevations for the step velocity when $\rho=0.8$, $h=0.1$, $T_1=2\times10^{-6}$ (Solid), $T_1=2\times10^{-4}$ (Dash), $T_1=2\times10^{-2}$ (Dash-Dotted), and $T_2=2T_1$

tonically decrease with surface tension. The contact-line elevation for the interface appears to be more involved than that for the free surface. Within the time shown it does not seem to converge to a terminal value, but rather continues to oscillate with a multiple wave motion (short waves on top of a longer wave). It is also to be noted that the time for the maximum elevation decreases with surface tension, in contrast to that for the free surface.

6. Flows Due to Harmonic Wavemaker Velocity

A wavemaker motion of greater practical interest is a periodic oscillation, for which the velocity of the wall is given as

$$U(t)=V\sin\left[\left(\frac{h}{g}\right)^{\frac{1}{2}}\Omega t\right],\quad t=0 \tag{61}$$

The Froude number is defined as in the previous section, and the normalization of the wavemaker velocity gives

$$u(t)=\sin\omega t \tag{62}$$

where the non-dimensional frequency of the wavemaker oscillation is $\omega=\Omega(h/g)^{1/2}$. The initial conditions are then

$$A(k,0)=0 \tag{63}$$

$$A_t(k,0)=-\frac{2\omega}{\pi k^2\lambda\cosh k}\left[1-\rho+\frac{\rho}{\cosh kh}\right] \tag{64}$$

$$A_{tt}(k,0)=0 \tag{65}$$

$$\begin{aligned}A_{ttt}(k,0)=&-\frac{2\omega^3(\rho-1)}{\pi k^2\lambda\cosh k}-\frac{2\omega^3\rho}{\pi k^2\lambda\cosh k\cosh(kh)}-\frac{2\omega\gamma_1(\rho+1)\tanh k}{\pi k\lambda^2\cosh k}\\&-\frac{2\omega}{\pi k\lambda^2\cosh k}\left[\gamma_2\tanh k(\rho^2\tanh^2(kh)-\rho^2-\rho\tanh^2(kh)+1)\right]\\&-\frac{2\omega\rho[\gamma_2(\rho\tanh k+\tanh(kh))+\gamma_2\tanh k]}{\pi k\lambda^2\cosh k\cosh(kh)}\end{aligned} \tag{66}$$

In Fig. 9, the configurations of the free surface and the interface are plotted for four different thickness ratios while other parameters, including the frequency $\omega=1$, are fixed. Wave fronts with decaying amplitudes far away from the wavemaker are reminiscent of the initial startup process, and the wave motions with relatively regular amplitudes that follow are consistent with the forcing frequency of the wavemaker. As h increases a secondary development of wave motions for the interface near the wavemaker is seen clearly, which is supposedly analogous to the secondary development of wiggles in the previous section. This secondary wave has higher frequency than that of the wavemaker. It is also interesting to note that unless the upper layer is sufficiently thick it is likely to rupture, as seen in figures (a), (b), and (c). As the upper-layer thickness increases the wave amplitudes at the interface decrease, making it less likely to rupture, as seen in figure (d).

In Fig. 10, the thickness ratio is fixed at $h=2$, and the density ratio is varied instead. Fig. 10(c) thus is identical to Fig. 9(d). Given the same thickness, the wave amplitudes at the free surface

and the interface decrease with the density ratio, and the rupture becomes less likely. It must be noted here that the secondary wave development at the interface disappears as the density ratio approaches either zero or unity. It is easily understood if we realize that either limit represents a single-layer system.

The contact-line elevations for the interface and the free surface are plotted in Fig. 11 as for other wavemaker motions in the previous sections. Perfectly harmonic oscillations are shown for both contact-lines. In all cases tried (not shown here) the contact line for the free surface always stays higher in position than that for the interface, so that no pinching, or rupture, is observed on the wavemaker.

Flows induced by an arbitrary motion of the wavemaker can be easily analyzed by a linear superposition of the solution for the harmonic velocity. An arbitrary wavemaker velocity can be approximated by a finite Fourier sine series

$$u(t)=\sum_{i=1}^{N} a_i \sin i\omega t \tag{67}$$

where N is a sufficiently large integer. For a single-layer wavemaker problem Joo et al.(1990) constructed a solution for the free-surface configuration with the wavemaker motion taken from that for a wave tank experiment. The solution was favorably compared with the experimental data.

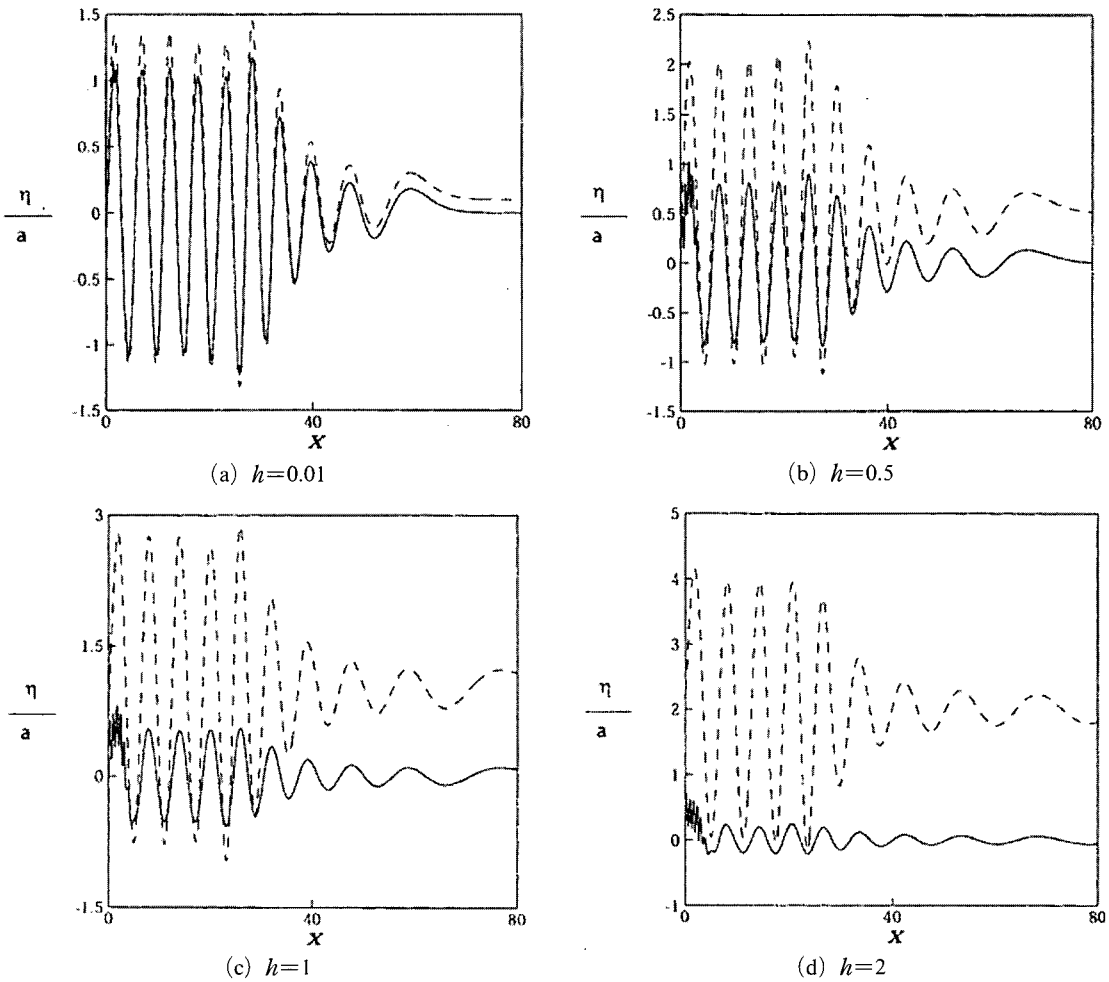

Fig. 9 Surface configurations for the harmonic velocity at $t=60$ when $\rho=0.8$, $\omega=1$, $T_1=2\times10^{-6}$, and $T_2=2$ T_1. For the interface (Solid) and the free surface (Dash)

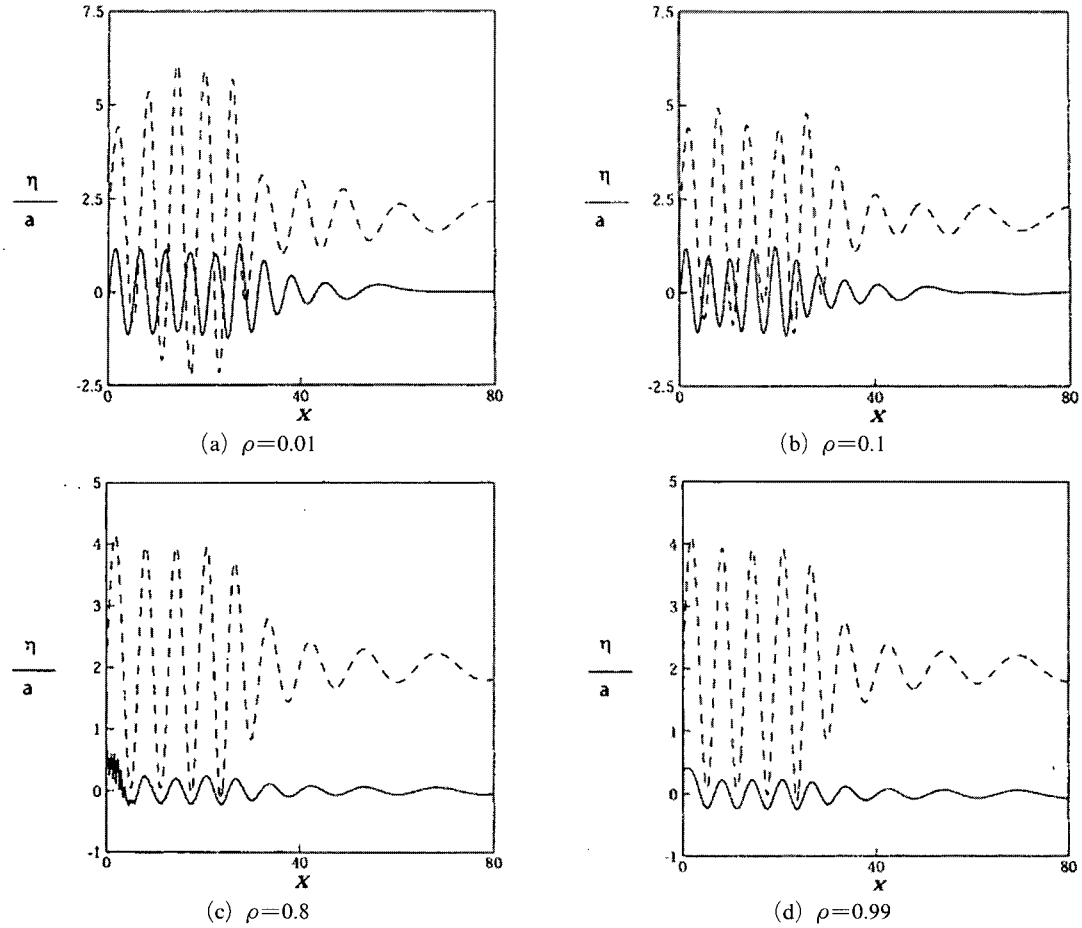

Fig. 10 Surface configurations for the harmonic velocity at $t=60$ when $h=2$, $\omega=1$, $T_1=2\times10^{-6}$, and $T_2=2$ T_1. For the interface (Solid) and the free surface (Dash)

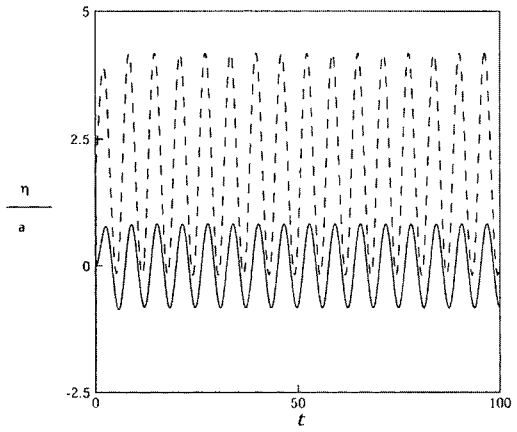

Fig. 11 Contact-line elevations for the harmonic velocity when $\rho=0.8$, $h=2$, $\omega=1$, $T_1=2\times10^{-6}$, and $T_2=2T_1$. For the interface (Solid) and the free surface (Dash)

For flows with two layers the same degree of accuracy can be expected in principle.

7. Concluding Remarks

Flows generated by a vertical wavemaker are studied for two vertically stratified horizontal layers. The solution method applied yields uniformly valid solutions for the transient free surface and interface configurations. Useful results are obtained with the inviscid and the small-Froude-number approximations.

It is generally known that viscous effects are confined to small areas near boundaries in studies of water waves, and so the inviscid approximation is proven to provide satisfactory results. Inclusion of viscous effects, including the shear stress on

rigid body and interfaces, invites the viscous moving-contact-line complications, and is not pursued in the immediate future. The small-Froude-number restriction, however, needs to be relaxed for practical applications. A new method that facilitates a parametric study on the Froude number must be sought. If one decides to use a computational method, extreme care must be exercised near the contact line, where a single length scale (thus the spatial resolution) and an explicit time integration may break down.

References

Chang, A. T., 1983, "Nonlinear Hyrodynamic Pressure on an Accelerating Plate.," *Phys. Fluids.*, 25, pp. 383~387.

Gradshteyn, I. S. and Ryzhik, I. M., 1980, Table of Integrals, Series, and Products., Academic Press.

Joo, S. W., Schultz, W. W. and Messiter, A. F., 1990, "An Analysis of the Initial-value Wavemaker Problem," *J. Fluid Mech.*, 214, pp. 161~183.

Joo, S. W. and Park, C. H., 2005, "An Initial-value Wavemaker Problem for a Stratified Fluid with Infinite Depth," Pending Publication.

Lin, W. M., 1984, "Nonlinear Motion of the Free Surface Near a Moving Body," Ph.D. Thesis, MIT, Dept. of Ocean Engineering.

Peregrine, D. H., 1972, "Flow Due to a Vertical Plate Moving in a Channel," Unpublished Note.

Rhodes-Robinson, P. F., 1994, On Wave Motion in a Two-layered Liquid of Infinite Depth in the Presence of Surface and Interfacial Tension," *J. Austral. Math. Soc. Ser. B*, 35, pp. 302~322.

Roberts, A. J., 1987, "Transient Free-surface Flows Generated by a Moving Vertical Plate," *Q. J. Mech. Appl. Maths.*, 40 pp. 129~158.

Sherief, H. H., Faltas, M. S. and Saad, E. I., 2003, "Forced Gravity Waves in Two-layered Fluids with the Upper Fluid Having a Free Surface," *Can. J. Phys.*, 81, pp. 675~689.